Published in final edited form as:
Proteins. 2011 February ; 79(2): 402–416. doi:10.1002/prot.22891.

A differential association of Apolipoprotein E isoforms with the Aβ oligomer in solution

Jitka Petrlova[1], **Hyun-Seok Hong**[2], **Daniel Bricarello**[3], **Ghimire Harishchandra**[5], **Gary Lorigan**[5], **Lee-Way Jin**[2], and **John C. Voss**[1,*]

[1]Department of Biochemistry & Molecular Medicine, University of California Davis, CA, USA

[2]M.I.N.D. Institute and Department of Pathology & Laboratory Medicine, University of California Davis, CA, USA

[3]Department of Applied Science, University of California Davis, CA, USA

[5]Department of Chemistry & Biochemistry, Miami University, Oxford, OH, USA

Abstract

The molecular pathogenesis of disorders arising from protein mis-folding and aggregation is difficult to elucidate, involving a complex ensemble of intermediates whose toxicity depends upon their state of progression along distinct processing pathways. To address the complex mis-folding and aggregation that initiates the toxic cascade resulting in Alzheimer's disease, we have developed a TOAC spin-labeled Aβ peptide to observe its isoform-dependent interaction with the apoE protein. While most individuals carry the E3 isoform of apoE, approximately 15% of humans carry the E4 isoform, which is recognized as the most significant genetic determinant for Alzheimer's. ApoE is consistently associated with the amyloid plaque marker for Alzheimer's disease. A vital question centers on the influence of the two predominant isoforms, E3 and E4, on Aβ peptide processing and hence Aβ toxicity. We employed EPR spectroscopy of incorporated spin labels to investigate the interaction of apoE with the toxic oligomeric species of Aβ in solution. EPR spectra of the spin labeled side chain report on side chain and backbone dynamics, as well as the spatial proximity of spins in an assembly. Our results indicate oligomer binding involves the C-terminal domain of apoE, with apoE3 reporting a much greater response through this conformational marker. Coupled with SPR binding measurements, apoE3 displays a higher affinity and capacity for the toxic Aβ oligomer. These findings support the hypothesis that apoE polymorphism and Alzheimer's risk can largely be attributed to the reduced ability of apoE4 to function as a clearance vehicle for the toxic form of Aβ.

Keywords

Alzheimer's disease; Apolipoprotein E; apoE isoforms; amyloid β-peptide; TOAC spin label; EPR spectroscopy

INTRODUCTION

Apolipoprotein E (apoE) is a 299 residue lipid binding protein that plays a main role in the metabolism and transport of cholesterol and lipids in the blood plasma and in the brain. ApoE is the predominant lipoprotein in the brain and is mainly synthesized and secreted by

*Address *correspondence to*: John C. Voss Department of Biochemistry & Molecular Medicine, School of Medicine University of California Davis, CA, USA; Tel.: 530 574 7583; Fax: 530 752 3516; jcvoss@ucdavis.edu.

astrocytes but also by microglia. ApoE can exist in a lipid free or lipid bound state, with the lipid-free state organized by two principal domains: a 22 kDa N-terminal domain and 10 kDa C-terminal domain. Although more than one lipid-bound conformation of the protein is likely 1›2, the lipid-bound protein is distinguished from the globular lipid-free structure as largely elongated α-helices that associate with the surface of the lipid particle. In humans, ApoE has three different isoforms, E3 is the most common one with an incidence of 78%. E4 has an incidence of 15% and E2 of 7%. The difference between these isoforms is a change at the 112 and 158 positions in the N- terminal domain. ApoE3 has cys/arg, apoE4 arg/arg and apoE2 cys/cys. ApoE is associated with age related risk for Alzheimer's disease (AD) and plays an important role in the homeostasis of the amyloid-β (Aβ) peptide. Individuals with the allele for apoE4 have an increased risk for cardiovascular disease as well as an increased risk of late onset AD.

The Aβ peptide is released by sequential intramembranous proteolytic cleavage of the amyloid precursor protein (APP) located in the neuronal membrane. The cleavage of APP is done by α-, β- and γ- secretases. The cleavage and processing of APP can be divided into amyloidogenic and a non-amyloidogenic pathway. In the non-amyloidogenic pathway, APP is cleaved by α-secretases and subsequently cleaved by γ- secretases. The development of Alzheimer's disease is linked with the turnover of the amyloidogenic pathway, where an alternative cleavage of APP leads to the generation of Aβ peptide. Here, β-secreatase performs the initial cleavage, followed by γ-secretase cleavage generating peptides ranging from 38 to 43 AA in length. The most common length of Aβ is 40 AA ($A\beta_{1\text{-}40}$). While the amyloid plaques composed of aggregated Aβ are the pathological marker for AD, abundant evidence points to the oligomeric intermediate within the Aβ aggregation pathway as the toxic species 3¯5. Because the soluble Aβ oligomer (AβO) represents a transient species in solution, studies of the AβO structure, dynamics and interaction with other molecules or assemblies require approaches that provide information on freshly prepared sample in solution. We report here the application of a modified Aβ peptide containing the conformationally restricted spin probe, 2,2,6,6-tetramethylpiperidine-1-oxyl-4-amino-4-carboxylic acid (TOAC). TOAC is part of a tetrasubstituted alpha carbon that reports on the peptide's assembly status and interaction with other proteins.

The E4 isoform of apolipoprotein E (apoE4) is the only recognized genetic risk factor for late onset AD (for reviews see 6¯9). Most individuals are homozygous for apoE3 isoform, but ~15% of the population carries the E4 allele. The difference in the primary structure is a single amino acid, at position 112 (apoE4-arg, apoE3-cys). Structurally, this change in the primary sequence is known to decrease the stability of N-terminal helical bundle and promote an ionic interaction between the N- and C-terminal domains, which has been associated with the preference of E4 to bind VLDL over HDL 10. Several in-vitro studies have shown the direct interaction between ApoE and AβO in the lipid-free and lipid-bound states 11¯14.

The exact mechanism of the effects of apoE on the onset and progression of AD is not completely understood. The altered lipid binding and stability properties of apoE4 may amplify Aβ toxicity. ApoE4, independent of Aβ, induces neuronal death and forms large fibril-like assemblies 15. Another line of evidence follows the beneficial properties of apoE3, in that it promotes neurite outgrowth 16 and may act as a chaperone to facilitate Aβ clearance and degradation 17. An additional variable relates to the physical state of the apoE (lipid-free vs. lipid-associated), with conflicting studies on the isoform dependence of Aβ binding and plaque formation 18. For example, measurements show lipid-free apoE4 binds Aβ with a higher affinity than apoE3 and promotes fibrillization of Aβ 14›19. However, using lipid-associated apoE, Aβ preferences for both apoE3 11›20 and apoE4 21 have been reported.

Since oligomeric Aβ represents a dynamic intermediate along the fibrilization pathway, much of the ambiguity in the affinity and influence of apoE isoforms with Aβ can be attributed to the difficulty in observing the interaction in solution. In addition, previous efforts largely rely on immunoprecipitation or capturing SDS-resistant complexes of apoE-Aβ, which may shift binding equilibria from the SDS-free state. In this regard, electron paramagnetic resonance (EPR) spectroscopy of site-directed spin labels can be especially useful through its ability to probe molecular interactions in solution.

Molecular motions associated with the side chain and backbone fluctuations that are modulated by conversions in secondary, tertiary and quaternary structure fall within rates of 0.1-50 nsec, a time regime within the sensitivity of X-band EPR. In addition, the ability of EPR to detect dipolar interactions between nearby labels also provides a route to observe peptide assembly as it processes from small oligomers to the mature fibril. EPR spectroscopy of site-directed spin labels in Aβ has already been used to explain the arrangement of peptides in the intact fibril 22. While Aβ in the fibril displays ordered beta-amyloid packing 22›23, simulations of the monomer in solution predict largely disordered backbone 24-26. The higher level of disorder of the soluble peptide species complicated our previous efforts (not shown) to identify spectral differences from spin-labeled Cys residues introduced at different positions in nascent oligomers. The high side chain and back bone flexibility (disorder) under conditions promoting either monomers (see 22 for example) or small oligomers of the Aβ peptide make the Cys-labeled Aβ peptides less than ideal for resolving changes in the dynamics related to the global rotational diffusion of the peptide, such as that accompanying a monomer→ oligomer transition. In contrast to nitroxides attached to a Cys residue, the TOAC spin label provides a rigid incorporation of the nitroxide ring into the peptide backbone, where its motions are not governed in part by rotations of side chain bonds. We have therefore synthesized TOAC-labeled Aβ, in order to obtain a spin-labeled Aβ whose line shape directly reflects the peptide backbone dynamics 27.

One element of predicted order in the Aβ peptide is the VGSN turn stabilized by a salt bridge formed by the flanking residues D23 and K28 26›28. Thus, we synthesized $A\beta_{(1\text{-}40)}$ containing the paramagnetic TOAC residue in place of Ser26 ($A\beta^{(26TOAC)}$). This report demonstrates that $A\beta^{(26TOAC)}$ provides a moderately immobilized EPR spectrum that is informative upon changes in global rotation diffusion, such as that occurring with the key interaction of the peptide with apoE. Finally, we have also targeted spin labels into apoE to assess the structural consequences of AβO binding. Because native apoE3 contains a Cys residue at position 112, we employ an E3-like mutant (Cys112→Ser), which has previously been shown to have a higher (relative to apoE4) propensity to form an SDS-resistant complex with Aβ 29.

METHODS

Materials

9-Fluorenylmethyl-oxycarbonyl-O-succinimide (Fmoc-OSu) and all the amino acids were purchased from Novabiochem, San Diego, CA. Hexafluro-2-propanol (HFIP), triisopropylsilane (TIS), anisole, 30% ammonium hydroxide [NH_3 (aq.)], piperidine were purchased from Sigma-Aldrich, St. Louis, MO. 2,2,6,6-Tetramethylpiperidine-1-oxyl-4-carboxylic acid (TOAC) was purchased from Acros Organics, Belgium. Trifluoroacetic acid (TFA), (2-(7-Aza-1H-benzotriazole-1-yl)-1,1,3,3-tetramethyluronium hexafluoro-phosphate (HATU), diisopropylethylamine (DIEA), M-Methyl-Pyrrolidone (NMP), dichloromethane (DCM), Fmoc-Val resin (0.75 m mol/g), were purchased from Applied Biosystems, Foster City, CA. Acetic Anhydride (Ac_2O), methyl-tert–butyl ether, and Dimethyl Sulfoxide (DMSO) were purchased from Fisher Scientific, Pittsburgh, PA. The thio-reactive spin label,

(1-Oxyl-2,2,5,5-tetramethyl-Δ3-pyrroline-3-methyl) Methanethiosulfonate (MTS-SL) was a kind gift of Prof. Kalman Hideg.

Synthesis and purification of TOAC-labeled Aβ

Synthesis of TOAC spin label substituted amino acid in the backbone of $A\beta_{(1-40)}$ in the 26 position ($A\beta^{TOAC26}$). $A\beta^{TOAC26}$ peptide was synthesized via solid phase peptide synthesis method using Fmoc-protection chemistry in 433A Peptide Synthesizer (Applied Biosystems Inc., Foster City, CA). Fmoc-protected TOAC was synthesized as previously described 30. The preloaded Fmoc-Val Resin (0.75 m mol/g) was used for the synthesis and all amino acids were single coupled with HATU. The amino acid sequence of the peptide is shown below.

^{1}DAEFRHDSGYEVHHQKLVFFAEDVG^{26}**S**NKGAIIGLMVGGV^{40}V→ Aβ-40 (WT)

^{1}DAEFRHDSGYEVHHQKLVFFAEDVG^{26}**X**NKGAIIGLMVGGV^{40}V→ 26-TOAC Aβ-40

Where **X** represents the TOAC spin label

433A peptide synthesizer connected with a UV-detector (wavelength 301 nM) was used to monitor the Fmoc-removal from the N-terminus of the growing peptide. The modified version of 0.1mmol Fast Fmoc Chemistry protocol in the SynthAssist 2.0 Software from Applied Biosystems (Foster city, CA) was used for the optimal peptide synthesis. All amino acids were purchased in Fmoc protected as well as the side-chain protected forms to minimize the unnecessary reactions during synthesis.

The peptide resins (150-200 mg) were treated with a suitable cleavage mixture (8.5mL TFA, 0.5mL TIS, 0.5mL anisole and 0.5mL distilled water) in a vortexing water bath for 3 hrs to remove all the side chains and detach peptides from the resin beads. The resins were then removed by filtration. The filtrate was concentrated and the peptide was precipitated using ice-cold methyl tert-butyl ether. The precipitated peptide was collected by centrifugation and vacuum dried overnight. The crude peptide was first dissolved in minimal amount of DMSO and then diluted with 20% aqueous DMSO solution just before HPLC injection. The peptide was processed on an Amersham Pharmacia Biotech AKTA Explorer HPLC system supported by unicorn (version 3) software. The protein C-4 semi-prep column (Vydac cat. # 214TP1010, 10μm, 10mm × 250 mm) was employed for peptide purification. The HPLC solvent system comprises of H_2O with 0.1% TFA (Solvent A) and the mixture of 95% acetonitrile, and 5% water with 0.1% TFA (Solvent B). Since TFA converts nitroxide spin label into hydroxylamine form during peptide cleavage, the purified peptide was treated with 10 % aq. ammonia (3 hrs) to fully regenerate the nitroxide spin label. The peptide purity was confirmed to be about 98% by matrix assisted laser desorption ionization time of flight (MALDI-TOF)] mass spectrometry.

Preparation of Aβ oligomer

Aβ samples were prepared as described previously 31. Briefly, the solid $A\beta_{(1-40)}$ peptide (Bachem Cat # 1194.0001) was dissolved in Hexa-Fluoro-Iso-Propanol (HFIP, Sigma) to disrupt existing hydrogen bonds and generate monomeric Aβ. The HFIP solution was incubated at room temperature for one day to achieve a clear and colorless solution. HFIP was removed by SpeedVac. One day of use, a fresh 1 mM stock of wt and spin-labeled Aβ was prepared by dissolving the dried peptide in DMSO. Oligomeric samples were prepared by dilution of the DMSO stock solution into cold PBS buffer, pH 7.4 to total concentration 100 μM. For oligomeric samples examined by EPR, the spins were first diluted by mixing the DMSO stock solutions at a ratio of I part $A\beta^{(26TOAC)}$ to 3 parts wt $A\beta_{(1-40)}$ prior to final

buffer dilution. This dilution is sufficient to overcome line broadening of the EPR spectrum that occurs between proximal spins in samples made from 100% $A\beta^{(26TOAC)}$.

ApoE protein Cloning and Purification

The gene encoding h_apoE4 protein containing the W264->Cys (apoE4-W264C) substitution was cloned into the commercial vector pET151/D-Topo (Invitrogen, CA) according to manufacturer instructions. The N-terminal fusion tag was removed by introducing flanking BamHI sites by PCR mutagenesis, followed by BamHI digestion and then ligation, so that the first residue of apoE (Lys) in the expressed protein is preceded by the sequence amino acids M-G-S. To generate the apoE3-like protein containing the same Cys substitution at position 264, the R112->S mutation in the apoE4-W264C template was introduced by PCR mutagenesis. Fidelity of cloning and mutations were confirmed by DNA sequencing.

For protein expression, apoE4-W264C and apoE3-like-W264C were transferred to the BL21(DE3)AI Escherichia coli cells (Invitrogen, CA). One-liter of cells in LB broth were grown to mid-log phase at 37°. These were then induced with 0.1% arabinose, and incubated for an additional 4 hrs 37°C. The cells were harvested by centrifugation, and inclusions bodies isolated and washed as described previously 32. To purify the protein, washed inclusion bodies were dissolved in 8 M urea, 200 mM NaCl, and the sample filtered through a 0.2 micron filter and then chromatographed on a SuperDex 200 (Pharmacia) size exclusion column using a mobile phase of 8M urea, 200 mM NaCl, 10mM TRIS (pH 7.5) and 1mM EDTA. The fraction was then desalted using a SuperDex 200 column using a mobile phase of 8M urea, 10mM TRIS (pH 7.5) and 1mM EDTA and then bound to a mono-Q ion exchange column. The column was washed with 8M urea,10 mM TRIS (pH 7.5) and 1mM EDTA, and the protein eluted using a gradient of NaCl. The major fraction was then spin labeled with 0.4 mM MTS-SL containing 100 μM TCEP to maintain reduced disulfides for 30 min. The labeled protein was then re-folded by dialysis (Slide-A-Lyzer, Thermo Scientific) against 0.1M ammonium bicarbonate and then PBS buffer pH 7.4. The sample was concentrated using centrifugal spin concentrators with a molecular size cutoff of 30 kDa (Millipore), and the protein concentration determined using the Pierce BCA kit (Thermo Scientific, USA). Secondary structural analysis (see Supplemental Materials) of purified and spin-labeled apoE4 was determined by circular dichroism measurements at PrimeSyn Lab Inc., Hillsborough, NJ using a JASCO CD-75 spectrometer.

Human Plasma Samples

Healthy human subjects were recruited from the University of California, Davis campus, under approval by the Institutional Review Board of the University. The volunteers consumed a moderately high-fat meal (40% calories from fat) and blood was obtained by venipuncture into EDTA-containing tubes 3.5 hours after ingestion of the test meal s. The VLDL was isolated from the postprandial plasma according to the previously published protocol in 33. Briefly, the plasma was adjusted with mock plasma solution (ρ = 1.0063 NaCl, KBr, and EDTA) and then processed by ultracentrifugation for 18 hours at 40,000 rpm in a SW41 Ti swinging bucket rotor (Beckman Coulter, Sunnyvale, CA) at 14°C. The triglyceride-rich lipoprotein fraction (VLDL and chylomicrons) was collected and separated by ultracentrifugation at 25,000 rpm for 30 minutes at 14°C to isolate the VLDL. Following VLDL isolation, the remaining plasma was further processed by sequential density gradient ultracentrifugation to yield LDL and HDL. The plasma was first adjusted to ρ = 1.063 using stock density solution (ρ = 1.4744 NaCl and NaBr) for the LDL isolation. LDL was isolated by centrifugation for 18 hours at 40,000 rpm in a SW41 Ti swinging bucket rotor (Beckman Coulter, Sunnyvale, CA) at 14°C.

After the LDL was removed, the remaining plasma was adjusted to ρ = 1.21 using stock density solution. For the HDL isolation, the plasma was then centrifuged for another 18 hours at 40,000 rpm in a SW41 Ti rotor at 14°C. The HDL fraction was collected and dialyzed in Spectra/Por® membrane tubing (molecular weight cutoff 3,500; Spectrum Medical Industries, Los Angeles, CA) at 4°C overnight against a saline solution containing 0.01% EDTA. Concentrated lipid samples were combined with the apoE and AβO for the EPR experiments.

Surface Plasmon Resonance

Surface Plasmon resonance (SPR) data were acquired on a BIAcore 3000 (Biacore Inc. Piscataway, NJ), equipped with four flow cells on a sensor chip, was use for determination of real time biding experiments. HBS-EP buffer was used as an assay running buffer and also for a sample preparation. A streptavidin sensor chip (Biacore Inc., Piscataway, NJ) in a flow cell was first saturated with biotinylated AβO. The binding of injected apoE3 and apoE4 with the immobilized AβO was revealed in the biosensorgrams. Typical SPR response curves are elicited by indicated apoE with a series of concentrations from 0.2 – 2 uM. The dissociation equilibrium constant KD (M), was obtained by calculating kd(s^{-1})/ ka($M^{-1}s^{-1}$) using Scrubber software (Hong et all., 2008).

EPR Spectroscopy

EPR measurements were carried out in a JEOL TE-100 X-band spectrometer fitted with a loop-gap resonator was used for EPR measurements as described previously 34. AβO was added to the spin-labeled protein (1-0.5 mg/mL) at a final concentration of 50-100 uM and use immediately for EPR measurements. Appropriate vehicle controls were used for all samples. Approximately 5 μl of the protein, at a final concentration of 30 μM was loaded into a sealed quartz capillary tube. The spectra were obtained by averaging two 2 minutes scans with a sweep width of 100 G at a microwave power of 4 mW and modulation amplitude optimized to the natural line width of the attached spin probe. All the spectra were recorded at room temperature.

To evaluate the contribution of global tumbling to the motional averaging of the EPR spectrum, the rotational correlation times (τ_c) were estimated using the Stoke's-Einstein-Sutherland relationship for diffusion rates by a spherical particle:

$$\tau_c = \frac{V_m \eta}{kT} \tag{1}$$

where η is the viscosity in P (cgs) and *k* and *T* have their usual meaning. The hydrated volume of a peptide can be approximated from:

$$V_m = \left(\text{protein spec vol}/6 \times 10^{23}\right)(\text{molec size in Da}) \tag{2}$$

where a value of 0.73 cm^3/g was used as the specific volume for a typical protein 35. Since it is unlikely the shape of either the peptide monomer or oligomer approximates a sphere, the predicted rates represent lower limits of τ_c. Solution viscosity was increased with the addition of the nonionic polymer, Ficoll-400. Samples containing ficoll-400 (Fisher BioReagents) were prepared by mixing a 60% stock solution of ficoll-400 (dissolved in either aqueous or DMSO solvent) with an equal volume of sample to provide a final ficoll level of 30%. The viscosity of a 30% ficoll solution (25° C) is 65.1 cP, as measured by the Brookfield method (Intertek Plastics Technology Laboratory, Pittsfield, MA).

EPR Spectral Simulation

EPR spectra were preprocessed using Wiener Noise filter 36,37 to improve signal-to-noise ratio. Spectral simulation was performed using NLSL data analysis program developed by Budil et al. 38,39. An isotropic Brownian diffusion motion was used to model the rotational motion of the system. The fixed optimized values of static magnetic parameters (g_{xx}=2.0093, g_{yy}=2.0071, g_{zz}=2.0024, A_{xx}=6.5362G, A_{yy}=6.8758G, A_{zz}=34.7069G) were used during the simulation of both monomer and oligomer spectra. The best-fit isotropic diffusion parameter (R) was extracted to calculate the correlation time (|$_c$) given by an expression, $\tau_c = \frac{1}{6R}$. The rotational correlation times were obtained as 1.3 ns for monomer and 7.1 ns for oligomer indicating that the motion of monomer is about six times faster than that of oligomer.

Fluorescence microscopy

Fluorescence microscopy imaging of $A\beta_{(1\text{-}40)}$βor $A\beta^{(26TOAC)}$ stained with 1-fluoro-2,5-bis-(3-hydroxycarbonyl-4-hydroxy)styrylbenzene (FSB), a dye that preferentially associates with amyloid protein assemblies, was carried out on a sample of 50 μM peptide in PBS following a 24 hr incubation as described previously 40.

MTT-FE assay

Toxicity of Aβ samples to the neurobrastoma cell line was determined using the colorimetric MTT (3-(4,5 dimethylthiazol-2yl)-2,5-diphenyltetrazolium bromide) assay as previously described 31. The cells were treated with oligomeric $A\beta_{(1\text{-}40}$ and $A\beta^{(26TOAC)}$ according to a previously published protocol in 31.

Atomic force microscopy

Atomic force microscopy (AFM) to analyze the oligomer formation of $A\beta_{(1\text{-}40)}$ and $A\beta^{(26TOAC)}$ was carried out as described previously 31. All surface scans employed a Dimension 3100 Scanning Probe Microscope with a Hybrid closed-loop XYZ head and Nanoscope IVa controller (Vecco, Santa Barbara, CA). All samples were prepared on freshly-cleaved mica (Ted Pella, Redding, CA) and imaged in tapping mode in air by a phosphorous-doped silicon cantilever with a nominal spring constant of 40 N/m. Particle dimension measurements and image enhancement were performed with the Nanoscope software supplied by Veeco, version 6.14. For each measurement, an aliquot of AβO was removed from 1 mM DMSO stock solution and diluted into 50 μM of AβO in PBS pH 7.4, and spotted on freshly clean mica at t=0 and t=1 hour incubation. After 2 minutes the samples were washed with 200 μl distilled water and then partially dried by compressed air and completely dried at room temperature. Assuming a simple spherical particle, the average volume of the initial AβO species from a set of 11 was 203 ± 26 nm^3. If packed similar to a globular protein, this would represent ~160 kD of protein mass 41, translating into ~35 monomers per oligomer. Given the high degree of disorder in the small AβO, efficient packing of the peptide in the particle is unlikely, thus a 30-mer represents an upper limit.

RESULTS

Placement of TOAC spin label in $A\beta_{(1\text{-}40)}$

To explore whether apoE isoforms have a differential interaction with oligomers of the $A\beta_{(1\text{-}40)}$ peptide, we designed solution EPR experiments to examine nitroxide spin labels located in Aβ, apoE, or both. EPR provides more than one perspective in which to analyze this interaction. First, small (hexamers or smaller) oligomers of $A\beta_{(1\text{-}40)}$ will have a molecular size under 25 kDa, low enough that perturbation of the global tumbling rate upon an increase or decrease in the molecular volume will influence the EPR line shape.

Secondly, binding is expected to be accompanied by stabilization of side chain or backbone dynamics, which may also be apparent as a change in the spectral line shape. Thirdly, a dipolar interaction between labels located on both $A\beta_{(1-40)}$ and apoE proximal to one another can be used to map the location of a binding interface. Due to the inherent disorder of Aβ in its soluble form (monomers or small oligomers), we selected the TOAC label for monitoring changes in the peptide's molecular dynamics. Thus, we synthesized $A\beta_{(1-40)}$ containing the paramagnetic TOAC residue in place of Ser26 ($A\beta^{(26TOAC)}$; Figure 1). Position 26 was selected due to its central location and the likelihood that this region retains some order, even in the monomeric state. Specifically, the central region of Aβ adopts a hairpin in the fibril [24,42] and most simulations predict this feature is favored from the monomer→mature fibril stage [24,26,28,42,43].

Behavior of TOAC-substituted Aβ

Because the oligomeric state of Aβ is key to its pathogenicity, we first determined whether $A\beta^{(26TOAC)}$ forms the oliogomeric state similarly to native $A\beta_{(1-40)}$, which we have previously established by multiple methods including microscopy, AFM, amyloid staining, and binding to an oligomer-specific antibody 44. To compare the assembly behavior of $A\beta^{(26TOAC)}$ to native $A\beta_{(1-40)}$, we first allowed the two peptides to aggregate over several hours and examined the characteristic amyloid structure that is readily detected by amyloid-sensitive dyes such as FSB 40. As shown in Figure 2A, for the identical amount of incubated peptide, the FSB-positive signal from the $A\beta^{(26TOAC)}$ is similar to that of native $A\beta_{(1-40)}$. This suggests that $A\beta^{(26TOAC)}$ retains the ability to form amyloid assemblies within 24 hours.

To examine the properties of the small oligomers formed by $A\beta^{(26TOAC)}$ relative to native $A\beta_{(1-40)}$, we examined the peptide samples by AFM on samples immediately spotted and following a 1-hr incubation. The results in Figure 2B demonstrate that the $A\beta^{(26TOAC)}$ peptide forms oligomers at a comparable rate and morphology to native $A\beta_{(1-40)}$.

The functional properties of $A\beta^{(26TOAC)}$ were investigated by assaying the peptide's toxicity to a neuronal cell line N2a 31 one day after addition of exogenous peptide to the culture. It was previously reported that Aβ aggregates (AβO) but not un-aggregated Aβ show potent toxicity to a neuroblastoma cell line, N2a 44. Figure 3 shows $A\beta^{(26TOAC)}$ is toxic to the N2a cells, displaying a similar potency as the native peptide, with the cell death ranging from 60-75%, and a non-detectable variability between two peptides. In summary, the staining, oligomeric and toxicity properties of $A\beta^{(26TOAC)}$ mirror that of the native $A\beta_{(1-40)}$ peptide, demonstrating that this derivative behaves functionally and structurally similar to the native peptide.

EPR analysis of TOAC-labeled Aβ

Dynamics of the nitroxide reorientation within the X-band EPR time scale (10^{-10} - 10^{-8} sec) are reflected in the width of the EPR spectrum. Since a near homogenous solution of monomeric Aβ is expected for HFIP-treated (see Methods) peptide freshly dissolved in DMSO, we measured the EPR spectrum of $A\beta^{(26TOAC)}$ under these conditions to determine the upper limit of global rotational averaging of the hyperfine anisotropy. To minimize the possible influence of dipolar broadening to the EPR spectrum, all EPR samples containing $A\beta^{(26TOAC)}$ were diluted 1:3 with native peptide ($A\beta^{(26TOAC)}$: $A\beta_{(1-40)}$). As shown in Figure 4, it is notable that even under these conditions, the spectrum is no more narrow than would be expected for a ~4.4 kD sample whose motional averaging is dominated by the peptide's global rotational tumbling, which should be on the order of a nanosecond. The optimized fit of the Aβ monomer spectrum (see inset to Figure 4A) predicts a rotational correlation time (τ_C) of 1.3 nsec, a rate appropriate for a molecule of this size. Thus, the

peptide backbone about position 26 is not highly disordered in these solvent conditions. Under conditions producing the oligomer species (i.e. one-hr in PBS buffer; see Fig. 2B and 44), the spectrum displays considerable broadening, as would be expected following a large increase in the rate of global rotational diffusion. It is unlikely that a significant fraction of monomeric $A\beta^{(26TOAC)}$ exists in this sample, as a rapidly diffusing monomeric population disproportionately contributes to the EPR spectrum.

Since the oligomeric species are predicted to consist of a molecular size greater than 30 kDa as imaged by various methods 31›44, the global tumbling of the species should have little influence on the EPR line shape. In contrast, global tumbling will have a major influence on monomeric Aβ (MW~4.4 kD), providing the spin label is at least moderately immobilized in the local structure. Therefore, we studied these samples under monomeric (DMSO) and oligomeric (1 hr, aqueous buffer) conditions in the presence and absence of 30% ficoll, a long chain neutral carbohydrate polymer of ~400,000 kD. Since the long polymer of ficoll will not solvate the side chain or backbone atoms, the change in the EPR line shape of the peptide in DMSO can be attributed to an altered rate of global tumbling.

As shown in Figure 4C, 30% ficoll has little effect on the $A\beta O^{(26TOAC)}$ spectrum, indicating that the orientational averaging due to global tumbling of the oligomeric species has no significant contribution to the observed line shape in buffered solution. However, under conditions that maintain monomeric peptide (DMSO), addition of 30% ficoll has a major effect on the line shape (Fig. 4B). Thus as expected, global tumbling of the monomer contributes to the narrow line shape of the peptide in DMSO. Based on the size of the monomeric $A\beta^{(26TOAC)}$ (4440 Da), the predicted rotational correlation time (τ_C) for global tumbling is on the order of 1.3 nsec. For the same-sized molecule, the predicted τ_C increases to ~88 nsec when the viscosity of the solution is dramatically increased to 0.65 P by inclusion of 30% ficoll. Absent any backbone flexibility, this longer τ_C would produce well-defined, broad splittings at the hyperfine extrema. However, this is not observed, and ficoll spectra for both monomer and oligomer Aβ resemble the oliogomer in the absence of ficoll. Thus, the motional narrowing of the monmeric $A\beta^{(26TOAC)}$ spectrum in 30% ficoll can be attributed to a moderate level of local backbone disorder. Simulation of the oligomer spectrum (see inset to Figure 4A) calculates the rate of this motion at 7.1 nsec.

The effects of solution viscosity on the oligomeric peptide were also determined. In this case, increasing the solution viscosity had no influence on the EPR line shape. Thus, the rotational diffusion of the oligomeric peptide does not contribute to the motional narrowing of the EPR spectrum at low viscosity, supporting the notion that this species has a molecular volume greater than 30 kDa. The absence of an effect due to the increased viscosity therefore indicates that any monomeric species (which display a more prevalent narrow line shape) in equilibrium with the oligomer represent a minor fraction in this preparation.

Interaction of apoE with oligomeric Aβ in solution

To probe the molecular basis of how the apoE4 isoform increases the risk for developing AD, we introduced a spin label into the C-terminal domain (position 264) of apoE, which represents the principle lipid binding domain and has been implicated in Aβ binding 45. As shown previously, the substitution and subsequent modification of the W264C mutant of apoE with the thiol-specific spin label does not alter its predicted distribution among plasma lipoproteins 46, and CD analysis of the labeled protein is indistinguishable from wt apoE4 (see Supplementary Material).

Because apoE3 is distinguished by a Cys residue at position 112, thiol-specific labeling to the C-terminal domain was carried out on an E3-like mutant (Cys112→Ser). This mutation was previously introduced into apoE4 by Bentley et al, 2002, to measure the influence on

binding to β amyloid by western blotting of SDS-resistant complexes. In an earlier study, we demonstrated via a similar approach that the disruption of the ionic interaction between the N- and C-terminal domains in an E3-like protein leads to a conformational change that can be observed by site-directed spin labels 47. These findings showed greater interaction of the C-terminal domain with the N-terminal domain is found in apoE4 compared to a mutant protein that behaves functionally similar to apoE3 47. Here, employing the E3-like Cys112→Ser mutation, a similar increase in the dynamics of a spin label targeted to the C-terminal domain is observed relative to the E4 protein, which contains an Arg at position 112. These results are shown in Figure 5. In this experiment, the EPR line shape of the nitroxide attached to position 264 in apoE4 is compared to the same position in the context of the Arg112→Ser mutation. Both proteins display two-component spectra, although the more dynamic species represents only a minor population in apoE4 (Fig. 5A, black traces). In contrast, and consistent with a less ordered environment, the spectrum of position 264 shows major narrow (dynamic) component in the E3-like protein. Thus the neutralization of Arg112 in our E3-like protein results in a more mobile C-terminal domain, just as predicted.

We then compared the consequences of adding AβO to spin-labeled apoE4 and the E3-like protein. The red traces in Figure 5A show the response to AβO binding. For each isoform, AβO broadens the spectrum, an indicator of dipolar coupling among the labels located at position 264 that reports the clustering of C-terminal domains from two or more apoE proteins 2‚46-49.

However, the effect of AβO is significantly greater for the E3-like protein, suggesting that AβO has a preference for the more dynamic population within the E3-like sample. The concentration dependence of the AβO-induced line broadening is shown in Figure 5B. Non-linear regression for the rate of change in spectral broadening produces apparent K_D values of 21 and 27 μM for apoE3-like and apoE4, respectively. Interestingly, the magnitude of the AβO-induced spectral change remains higher for the E3-like protein even at higher concentrations where the effect saturates in both isoforms. The fact that change in EPR amplitude for apoE4 saturates at a lower AβO levels (despite having a lower affinity for AβO) suggests apoE3 has a higher capacity for AβO binding, which may correlate to a higher affinity for AβO (see Figure 8 below).

To explore whether the differential effects of AβO carried over to the lipid-bound state, similar experiments were repeated in the presence of postprandial plasma (Fig. 6). As demonstrated earlier, nearly all of the exogenous apoE added to postprandial plasma becomes lipid bound 46. βO also induces greater C-terminal domain interaction in apoE3 when combined with postprandial plasma. This suggests the differences in Aβ (and subsequent conformational differences) are carried over to the lipid-bound state.

The ability of plasma lipids to enhance the effect of AβO on the E3-like spectrum points to a possible role of the class of lipid to which apoE is associated, since E3 has a preference for HDL and E4 a preference for VLDL. Upon binding to either HDL or VLDL, the C-terminal domain of the E3-like protein (which lacks domain interaction in the lipid-free state) becomes more ordered; where the spectra of spin-labeled 264 are similarly broadened by HDL and VLDL (see Supplemental Figure S2). In contrast, apoE4 shows little change with HDL, and a slight increase in amplitude with VLDL (Supplemental Figure S2). The difference in the isoforms' response to the two lipid fractions is more pronounced in the presence of AβO, particularly for the E3-like protein on AβO-treated HDL (Figure 7). Thus, the influence of AβO on the E3-like protein is clearly greater in the presence of HDL, suggesting the HDL-bound form of the protein has a higher affinity for AβO and/or a greater propensity for self-association in the presence of AβO.

We have previously used surface plasmon resonance (SPR; 50 to measure the binding of fluorine compounds to immobilized AβO 44. Thus, we used this method to confirm the apparent higher affinity of the E3-like protein for AβO. Figure 8 shows the resulting SPR curves when either apoE4 or the E3-like protein is flowed over immobilized AβO. The calculated AβO affinity of the E3-like protein is ~3× greater than that of apoE4, with K_D values of 2.7×10^{-8} and $9.8*10^{-8}$, respectively. In each of four independent SPR measurements, the K_D value of the E3-like protein for AβO was 1/3 to 1/4 of apoE4, clearly reflecting that the E3 isoform has a higher affinity for the immobilized oligomer.

Spin-labels attached to monomeric Aβ also indicate a preference for the E3 isoform

The broad spectrum of the TOAC-labeled AβO assembly precludes our ability to detect changes in the global rotational diffusion of this body upon apoE binding. However, such changes should be evident in a preparation of Aβ monomers or smaller oligomers, where the TOAC spectrum is considerably sharper (see Figure 4A). To explore this, Aβ (1 part TOAC-26 : 3 parts native) from a freshly prepared DMSO solution was added to PBS buffer containing apoE and immediately scanned by EPR. Figure 9 compares the spectrum of a sample containing the E3-like protein to the spectrum of the sample containing apoE4. Only the E3-like protein induces a broadening of the $Aβ^{(26TOAC)}$ spectra, consistent with a tighter affinity for Aβ by this isoform. The sample containing apoE4 produces a spectrum that is identical to TOAC-labeled sample added to PBS alone (not shown).

DISCUSSION

AD is a multifactorial disease, and the influence of apoE on disease onset and progression likely results from its effect on more than a single process (reviewed in 7-9). Since apoE is always found to co-localize with Aβ deposits *in vivo*, much effort has focused on the association of apoE isoforms with Aβ. Initial efforts focused on the role of apoE isoforms on the formation of large amyloid assemblies (the amyloid burden as detected in plaques or fibrils), although an isoform-dependent linkage of amyloid burden and disease is not clear. For example, mouse models find profound, but opposite results on amyloid formation depending on whether human or mouse apoE is used 51.

In vitro and cell culture studies exploring the isoform dependence of apoE binding to Aβ have also not arrived at a single correlation between an isoform preference of Aβ and AD risk. *In vivo*, Aβ fibrils are always found to co-assemble with apoE3 or apoE3+apoE4 in carriers of the E4 allele. Although literature contains conflicting conclusions, in general studies on fibrils suggest a higher E4 association, while more recent studies find apoE3 has a higher avidity for the soluble oligomer of Aββ For example, *in vitro* assembly of Aβ fibrils is stimulated by apoE, and more so by the E4 isoform 19. Early *in vitro* measurements were in line with this correlation, finding the level of SDS-resistant apoE-Aβ detected on gels found higher apoE4 association *in vitro* 13. However when soluble particles are isolated from cell culture medium, a higher affinity for apoE3 was found 52. ApoE3 from human CSF was also found to form much higher levels of SDS-resistant complexes with added Aβ peptide when compared to apoE4, however the same group found no difference between the isoforms when the source was cell culture medium 53.

More recently, investigations of AD pathogenesis have focused on AβO, the smaller assemblies of Aβ, in that they display far greater toxicity to cultured neurons 21،44،54. Thus by viewing the amyloid fibril as a marker of increased Aβ generation or decreased Aβ clearance (rather than the pathogenic species), helps reconcile many of the divergent findings of earlier work. As elevated levels of Aβ progress to the fibril, they will co-assemble with either apoE3 or E4. It is possible that the fibril form of Aβ has a higher affinity for apoE4, and the higher propensity of apoE4 to convert to β-rich neurotoxic fibrils

on its own 15, suggests that apoE4 may more readily co-assemble in amyloid fibrils. On the other hand, the association of apoE3 with smaller oligomeric species may facilitate its exchange on lipoprotein particles at the blood brain barrier9. Focusing *in vitro* studies on a defined oligomeric species 11 should bring clarity to the problem by limiting protocols to the more clinically relevant system. In addition, apoE, and especially the E4 isoform has limited stability and complex aggregation propensities 15, properties that can greatly affect its structure and functionality. In this study, we focus on the differences of AβO binding affinity between apoE4 and the E3-like mutant Arg112->Ser, previously introduced by Bentley et. al. 29. Consistent with our earlier studies 2،47 using a different E3-mimic, the E3 like protein employed here displays greater motional freedom (relative to apoE4) at position 264 in the C-terminus. Thus, decreased order within the C-terminal domain of the E3-like protein reflects the hallmark structural distinction between the two isoforms: a lower level of domain interaction in apoE3 47.

A major obstacle in understanding how apoE influences the processing of the Aβ peptide in the brain has been the lack of an appropriate means to detect - in solution - the interaction of the two species. Previous studies which have used spin labeled side chains of substituted Cys residues to elucidate fibril formation 22 or the interaction of redox-active side chains within the hairpin 55 have found spectra displaying extremely mobile side chains for the soluble peptide. The TOAC-labeled Aβ synthesized for this purpose is particularly useful in that the probe is positioned in the more ordered region of the peptide. Importantly, we show that despite the unique constraints of the tetrasubstituted TOAC residue, incorporation at position 26 has no evident effects on Aβ toxicity and aggregation. Since TOAC has the propensity to disrupt β-strands and induce turns in peptides 56, its location near the predicted hairpin region of Aβ may represent an especially well-tolerated position within the peptide (Fig. 1). In addition, since soluble Aβ (monomers, oligomers) is highly disordered 22،25،28،55،57،58, the apparent higher order of the hairpin region also allows for a more motion-constrained EPR spectrum. This is significant because extreme disorder dominates the spectrum, masking even large changes in the rate of global tumbling in the EPR spectrum.

Previous work has implicated the C-terminal region of apoE in Aβ binding 13،19. A fundamental distinction between the two isoforms is the presence of domain interaction in apoE4, a feature involving the interaction of the C-terminal domain with the N-terminal helical bundle 10،47.

Domain interaction, while also accounting for stability and lipid-binding differences between the two alleles, may also account for the lower binding affinity of apoE4. It is helpful to point out that in the lipid-free state, domain interaction results in the C-terminal region of apoE4 displaying a higher level of order even though this isoform is less stable than apoE3 15،59. Since the presence of arginine at position 112 in apoE4 drives an electrostatic docking of the C-terminal domain with the helical bundle, this reduced C-terminal availability may explain the reduced binding affinity of apoE4 for AβO. This mechanism supports the hypothesis that a primary detriment of the apoE4 allele is that it has a poor ability to chaperone AβO through the normal clearance pathway.

The AβO-induced changes in apoE quaternary structure detected by EPR fall within the same micromolar range that result in neuronal cell toxicity. The nanomolar affinity of surface-immobilized AβO for apoE as measured by SPR is somewhat surprising. The AβO in the SPR experiments represents a covalently trapped form of the oligomer that may stabilize a favored conformation of AβO for apoE interaction, while the EPR measurements utilize a species in dynamic equilibrium. Since the EPR broadening parameter is reflecting the level of apoE oligomerization through the dipolar coupling of adjacent spin labels, it

should also be noted that the EPR parameter is reporting a secondary effect of AβO binding that may be more related to the capacity of each isoform to bind Aβ. Hence, the fact that the broadening of the apoE3-like protein saturates at a higher magnitude implies that AβO binding in solution may promote the formation of higher-ordered apoE oligomers (such as tetramers) dependent on micromolar amounts of Aβ. In the case of the E4 isoform, domain interaction may compete with this process limiting the total magnitude of broadening. This observation, combined with the SPR data, suggests that in addition to apoE3's higher affinity for AβO, a higher binding capacity may be equally important in its role to mitigate AβO toxicity.

The greater spectral perturbation seen with apoE3 upon AβO addition is amplified in the lipid-bound state, as is achieved by combining the protein with postprandial plasma, and even more so when the protein is bound to HDL. This response reflects a stronger affinity of apoE3 for AβO when the protein is docked on HDL, the plasma lipoprotein that most closely resembles the species found in brain. In addition, our results show a slightly stronger binding effect of apoE4 to AβO in the presence of VLDL than HDL. These findings are consistent with the notion that the lipid-bound apoE forms a tighter complex with Aβ. Furthermore, the finding that AβO induces the greatest spectral change to HDL-associated apoE3 is in line with the established distribution preferences of the isoforms (i.e., apoE3 for HDL, apoE4 for VLDL).

CONCLUSION

The recognition of AβO as the toxic species, and the development of protocols to generate a defined AβO species 11, provides a route to overcome much of the ambiguity remaining with respect to the association and pathological consequences of apoE and Aβ. The EPR approach is a valuable tool for investigating the interaction of apoE isoforms and AβO in aqueous environment, and the spectra report on both the dynamics and proximity of spin-labeled positions. Our approach can be extended to map the binding geometries within the ApoE and AβO complex. Future studies that target spin labels to additional positions in apoE will help uncover the geometries of AβO docked to apoE. This works provides support to the hypothesis [11,29] attributing the increased AD risk for carriers of the E4 allele is in part attributed to a diminished clearance of the AβO species.

Supplementary Material

Refer to Web version on PubMed Central for supplementary material.

Acknowledgments

We are grateful to Dr. Robin Altman for preparing the lipoprotein fractions and to Dr. Indra Sahu for NLSL fitting of EPR spectra. This work was supported by a grant form the U.S. National Institutes of Health (R01 AG029246).

REFERENCES

1. Gupta V, Narayanaswami V, Budamagunta MS, Yamamato T, Voss JC, Ryan RO. Lipid-induced extension of apolipoprotein E helix 4 correlates with low density lipoprotein receptor binding ability. The Journal of biological chemistry. 2006; 281(51):39294–39299. [PubMed: 17079229]
2. Hatters DM, Voss JC, Budamagunta MS, Newhouse YN, Weisgraber KH. Insight on the molecular envelope of lipid-bound apolipoprotein E from electron paramagnetic resonance spectroscopy. J Mol Biol. 2009; 386(1):261–271. [PubMed: 19124026]
3. Bharadwaj PR, Dubey AK, Masters CL, Martins RN, Macreadie IG. Abeta aggregation and possible implications in Alzheimer's disease pathogenesis. J Cell Mol Med. 2009; 13(3):412–421. [PubMed: 19374683]

4. Lesne S, Koh MT, Kotilinek L, Kayed R, Glabe CG, Yang A, Gallagher M, Ashe KH. A specific amyloid-beta protein assembly in the brain impairs memory. Nature. 2006; 440(7082):352–357. [PubMed: 16541076]
5. Klein WL, Stine WB Jr. Teplow DB. Small assemblies of unmodified amyloid beta-protein are the proximate neurotoxin in Alzheimer's disease. Neurobiology of aging. 2004; 25(5):569–580. [PubMed: 15172732]
6. Weisgraber KH, Mahley RW. Human apolipoprotein E: the Alzheimer's disease connection. Faseb J. 1996; 10(13):1485–1494. [PubMed: 8940294]
7. Raber J, Huang Y, Ashford JW. ApoE genotype accounts for the vast majority of AD risk and AD pathology. Neurobiology of aging. 2004; 25(5):641–650. [PubMed: 15172743]
8. Cedazo-Minguez A, Cowburn RF. Apolipoprotein E: a major piece in the Alzheimer's disease puzzle. J Cell Mol Med. 2001; 5(3):254–266. [PubMed: 12067484]
9. Hirsch-Reinshagen V, Wellington CL. Cholesterol metabolism, apolipoprotein E, adenosine triphosphate-binding cassette transporters, and Alzheimer's disease. Curr Opin Lipidol. 2007; 18(3): 325–332. [PubMed: 17495608]
10. Hatters DM, Peters-Libeu CA, Weisgraber KH. Apolipoprotein E structure: insights into function. Trends Biochem Sci. 2006; 31(8):445–454. [PubMed: 16820298]
11. Manelli AM, Stine WB, Van Eldik LJ, LaDu MJ. ApoE and Abeta1-42 interactions: effects of isoform and conformation on structure and function. J Mol Neurosci. 2004; 23(3):235–246. [PubMed: 15181252]
12. Tokuda T, Calero M, Matsubara E, Vidal R, Kumar A, Permanne B, Zlokovic B, Smith JD, Ladu MJ, Rostagno A, Frangione B, Ghiso J. Lipidation of apolipoprotein E influences its isoform-specific interaction with Alzheimer's amyloid beta peptides. The Biochemical journal. 2000; 2(348 Pt):359–365. [PubMed: 10816430]
13. Strittmatter WJ, Weisgraber KH, Huang DY, Dong LM, Salvesen GS, Pericak-Vance M, Schmechel D, Saunders AM, Goldgaber D, Roses AD. Binding of human apolipoprotein E to synthetic amyloid beta peptide: isoform-specific effects and implications for late-onset Alzheimer disease. Proceedings of the National Academy of Sciences of the United States of America. 1993; 90(17):8098–8102. [PubMed: 8367470]
14. Sanan DA, Weisgraber KH, Russell SJ, Mahley RW, Huang D, Saunders A, Schmechel D, Wisniewski T, Frangione B, Roses AD, et al. Apolipoprotein E associates with beta amyloid peptide of Alzheimer's disease to form novel monofibrils. Isoform apoE4 associates more efficiently than apoE3. J Clin Invest. 1994; 94(2):860–869. [PubMed: 8040342]
15. Hatters DM, Zhong N, Rutenber E, Weisgraber KH. Amino-terminal domain stability mediates apolipoprotein E aggregation into neurotoxic fibrils. J Mol Biol. 2006; 361(5):932–944. [PubMed: 16890957]
16. Nathan BP, Bellosta S, Sanan DA, Weisgraber KH, Mahley RW, Pitas RE. Differential effects of apolipoproteins E3 and E4 on neuronal growth in vitro. Science. 1994; 264(5160):850–852. [PubMed: 8171342]
17. Jordan J, Galindo MF, Miller RJ, Reardon CA, Getz GS, LaDu MJ. Isoform-specific effect of apolipoprotein E on cell survival and beta-amyloid-induced toxicity in rat hippocampal pyramidal neuronal cultures. J Neurosci. 1998; 18(1):195–204. [PubMed: 9412500]
18. Carter DB. The interaction of amyloid-beta with ApoE. Subcell Biochem. 2005; 38:255–272. [PubMed: 15709483]
19. Wisniewski T, Castano EM, Golabek A, Vogel T, Frangione B. Acceleration of Alzheimer's fibril formation by apolipoprotein E in vitro. Am J Pathol. 1994; 145(5):1030–1035. [PubMed: 7977635]
20. Wisniewski T, Frangione B. Apolipoprotein E: a pathological chaperone protein in patients with cerebral and systemic amyloid. Neurosci Lett. 1992; 135(2):235–238. [PubMed: 1625800]
21. Stine WB Jr. Dahlgren KN, Krafft GA, LaDu MJ. In vitro characterization of conditions for amyloid-beta peptide oligomerization and fibrillogenesis. The Journal of biological chemistry. 2003; 278(13):11612–11622. [PubMed: 12499373]

22. Torok M, Milton S, Kayed R, Wu P, McIntire T, Glabe CG, Langen R. Structural and dynamic features of Alzheimer's Abeta peptide in amyloid fibrils studied by site-directed spin labeling. The Journal of biological chemistry. 2002; 277(43):40810–40815. [PubMed: 12181315]
23. Petkova AT, Yau WM, Tycko R. Experimental constraints on quaternary structure in Alzheimer's beta-amyloid fibrils. Biochemistry. 2006; 45(2):498–512. [PubMed: 16401079]
24. Reddy G, Straub JE, Thirumalai D. Influence of preformed Asp23-Lys28 salt bridge on the conformational fluctuations of monomers and dimers of Abeta peptides with implications for rates of fibril formation. J Phys Chem B. 2009; 113(4):1162–1172. [PubMed: 19125574]
25. Tarus B, Straub JE, Thirumalai D. Dynamics of Asp23-Lys28 salt-bridge formation in Abeta10-35 monomers. Journal of the American Chemical Society. 2006; 128(50):16159–16168. [PubMed: 17165769]
26. Lazo ND, Grant MA, Condron MC, Rigby AC, Teplow DB. On the nucleation of amyloid beta-protein monomer folding. Protein Sci. 2005; 14(6):1581–1596. [PubMed: 15930005]
27. McNulty, JC.; Millhauser, GL. TOAC: The rigid nitroxide side chain.. In: Berliner, LJ.; Eaton, SS.; Eaton, GR., editors. Distance measurements in biological systems by EPR. Volume 19, Biological Magnetic Resonance. Plenum Press; New York: 2000. p. 277-307.
28. Baumketner A, Shea JE. The structure of the Alzheimer amyloid beta 10-35 peptide probed through replica-exchange molecular dynamics simulations in explicit solvent. J Mol Biol. 2007; 366(1):275–285. [PubMed: 17166516]
29. Bentley NM, Ladu MJ, Rajan C, Getz GS, Reardon CA. Apolipoprotein E structural requirements for the formation of SDS-stable complexes with beta-amyloid-(1-40): the role of salt bridges. The Biochemical journal. 2002; 366(Pt 1):273–279. [PubMed: 12015813]
30. Marchetto R, Schreier S, Nakaie CR. A Novel Spin-labeled Amino Acid Derivative for Use in Peptide Synthesis: (9-Fluorenylmethyloxycarbonyl)-2,2,6,6-tetramethylpiperidine-N-oxyl-4-amino-4-carboxylic Acid. J Am Chem Soc. 1993; 115:11042–11043.
31. Hong HS, Maezawa I, Yao N, Xu B, Diaz-Avalos R, Rana S, Hua DH, Cheng RH, Lam KS, Jin LW. Combining the rapid MTT formazan exocytosis assay and the MC65 protection assay led to the discovery of carbazole analogs as small molecule inhibitors of Abeta oligomer-induced cytotoxicity. Brain research. 2007; 1130(1):223–234. [PubMed: 17157826]
32. Hess JF, Voss JC, FitzGerald PG. Real-time observation of coiled-coil domains and subunit assembly in intermediate filaments. The Journal of biological chemistry. 2002; 277(38):35516–35522. [PubMed: 12122019]
33. Wang L, Gill R, Pedersen TL, Higgins LJ, Newman JW, Rutledge JC. Triglyceride-rich lipoprotein lipolysis releases neutral and oxidized FFAs that induce endothelial cell inflammation. Journal of lipid research. 2009; 50(2):204–213. [PubMed: 18812596]
34. Lagerstedt JO, Budamagunta MS, Oda MN, Voss JC. Electron paramagnetic resonance spectroscopy of site-directed spin labels reveals the structural heterogeneity in the N-terminal domain of apoA-I in solution. The Journal of biological chemistry. 2007; 282(12):9143–9149. [PubMed: 17204472]
35. Murphy LR, Matubayasi N, Payne VA, Levy RM. Protein hydration and unfolding--insights from experimental partial specific volumes and unfolded protein models. Fold Des. 1998; 3(2):105–118. [PubMed: 9565755]
36. Hornak JP, Moscicki JK, Schneider DJ, Freed JH. Diffusion Coefficients in Anisotropic Fluids by ESR Imaging of Concentration Profiles. J Chem Phys. 1986; 84:3387–3395.
37. Press, WW.; Teukolsky, SA.; Vetterling, WT.; Flannery, BP. Numerical Recipes in Fortran: The Art of Scientific Computing. Cambridge University Press; New York: 1992. p. 963
38. Budil DE, Lee S, Saxena S, Freed JH. Nonlinear-Least-Squares Analysis of Slow-Motion EPR Spectra in One and Two Dimensions Using a Modified Levenberg–Marquardt Algorithm. J Mag Reson Series A. 1996; 120:155–189.
39. Schneider, DJ.; Freed, JH. Calculating Slow Motional Magnetic Resonance Spectra: A Users's Guide.. In: Berliner, LJ.; Reuben, J., editors. Spin Labeling: Theory and Applications. Volume 8, Biological Magnetic Resonance. Plenum Press; NY: 1989. p. 1-76.

40. Sato K, Higuchi M, Iwata N, Saido TC, Sasamoto K. Fluoro-substituted and 13C-labeled styrylbenzene derivatives for detecting brain amyloid plaques. Eur J Med Chem. 2004; 39(7):573–578. [PubMed: 15236837]
41. Pietrasanta LI, Thrower D, Hsieh W, Rao S, Stemmann O, Lechner J, Carbon J, Hansma H. Probing the Saccharomyces cerevisiae centromeric DNA (CEN DNA)-binding factor 3 (CBF3) kinetochore complex by using atomic force microscopy. Proceedings of the National Academy of Sciences of the United States of America. 1999; 96(7):3757–3762. [PubMed: 10097110]
42. Lam AR, Teplow DB, Stanley HE, Urbanc B. Effects of the Arctic (E22-->G) mutation on amyloid beta-protein folding: discrete molecular dynamics study. Journal of the American Chemical Society. 2008; 130(51):17413–17422. [PubMed: 19053400]
43. Liu FF, Ji L, Dong XY, Sun Y. Molecular insight into the inhibition effect of trehalose on the nucleation and elongation of amyloid beta-peptide oligomers. J Phys Chem B. 2009; 113(32): 11320–11329. [PubMed: 19719268]
44. Hong HS, Maezawa I, Budamagunta M, Rana S, Shi A, Vassar R, Liu R, Lam KS, Cheng RH, Hua DH, Voss JC, Jin LW. Candidate anti-Abeta fluorene compounds selected from analogs of amyloid imaging agents. Neurobiology of aging. 2008
45. Reinhard C, Hebert SS, De Strooper B. The amyloid-beta precursor protein: integrating structure with biological function. Embo J. 2005; 24(23):3996–4006. [PubMed: 16252002]
46. Tetali SD, Budamagunta MS, Voss JC, Rutledge JC. C-terminal interactions of apolipoprotein E4 respond to the postprandial state. Journal of lipid research. 2006; 47(7):1358–1365. [PubMed: 16632798]
47. Hatters DM, Budamagunta MS, Voss JC, Weisgraber KH. Modulation of Apolipoprotein E Structure by Domain Interaction: DIFFERENCES IN LIPID-BOUND AND LIPID-FREE FORMS. The Journal of biological chemistry. 2005; 280(40):34288–34295. [PubMed: 16076841]
48. Zhang Y, Vasudevan S, Sojitrawala R, Zhao W, Cui C, Xu C, Fan D, Newhouse Y, Balestra R, Jerome WG, Weisgraber K, Li Q, Wang J. A monomeric, biologically active, full-length human apolipoprotein E. Biochemistry. 2007; 46(37):10722–10732. [PubMed: 17715945]
49. Fan D, Li Q, Korando L, Jerome WG, Wang J. A monomeric human apolipoprotein E carboxyl-terminal domain. Biochemistry. 2004; 43(17):5055–5064. [PubMed: 15109264]
50. Piliarik M, Vaisocherova H, Homola J. Surface plasmon resonance biosensing. Methods Mol Biol. 2009; 503:65–88. [PubMed: 19151937]
51. Holtzman DM, Bales KR, Tenkova T, Fagan AM, Parsadanian M, Sartorius LJ, Mackey B, Olney J, McKeel D, Wozniak D, Paul SM. Apolipoprotein E isoform-dependent amyloid deposition and neuritic degeneration in a mouse model of Alzheimer's disease. Proceedings of the National Academy of Sciences of the United States of America. 2000; 97(6):2892–2897. [PubMed: 10694577]
52. LaDu MJ, Falduto MT, Manelli AM, Reardon CA, Getz GS, Frail DE. Isoform-specific binding of apolipoprotein E to beta-amyloid. J Biol Chem. 1994; 269(38):23403–23406. [PubMed: 8089103]
53. Zhou Z, Relkin N, Ghiso J, Smith JD, Gandy S. Human cerebrospinal fluid apolipoprotein E isoforms are apparently inefficient at complexing with synthetic Alzheimer's amyloid-[beta] peptide (A[beta] 1-40) in vitro. Mol Med. 2002; 8(7):376–381. [PubMed: 12393935]
54. Kayed R, Head E, Thompson JL, McIntire TM, Milton SC, Cotman CW, Glabe CG. Common structure of soluble amyloid oligomers implies common mechanism of pathogenesis. Science. 2003; 300(5618):486–489. [PubMed: 12702875]
55. Murakami K, Hara H, Masuda Y, Ohigashi H, Irie K. Distance measurement between Tyr10 and Met35 in amyloid beta by site-directed spin-labeling ESR spectroscopy: implications for the stronger neurotoxicity of Abeta42 than Abeta40. Chembiochem. 2007; 8(18):2308–2314. [PubMed: 18022992]
56. Crisma M, Deschamps JR, George C, Flippen-Anderson JL, Kaptein B, Broxterman QB, Moretto A, Oancea S, Jost M, Formaggio F, Toniolo C. A topographically and conformationally constrained, spin-labeled, alpha-amino acid: crystallographic characterization in peptides. J Pept Res. 2005; 65(6):564–579. [PubMed: 15885116]

57. Sgourakis NG, Yan Y, McCallum SA, Wang C, Garcia AE. The Alzheimer's peptides Abeta40 and 42 adopt distinct conformations in water: a combined MD / NMR study. J Mol Biol. 2007; 368(5): 1448–1457. [PubMed: 17397862]

58. Zhang S, Iwata K, Lachenmann MJ, Peng JW, Li S, Stimson ER, Lu Y, Felix AM, Maggio JE, Lee JP. The Alzheimer's peptide a beta adopts a collapsed coil structure in water. J Struct Biol. 2000; 130(2-3):130–141. [PubMed: 10940221]

59. Morrow JA, Segall ML, Lund-Katz S, Phillips MC, Knapp M, Rupp B, Weisgraber KH. Differences in stability among the human apolipoprotein E isoforms determined by the amino-terminal domain. Biochemistry. 2000; 39(38):11657–11666. [PubMed: 10995233]

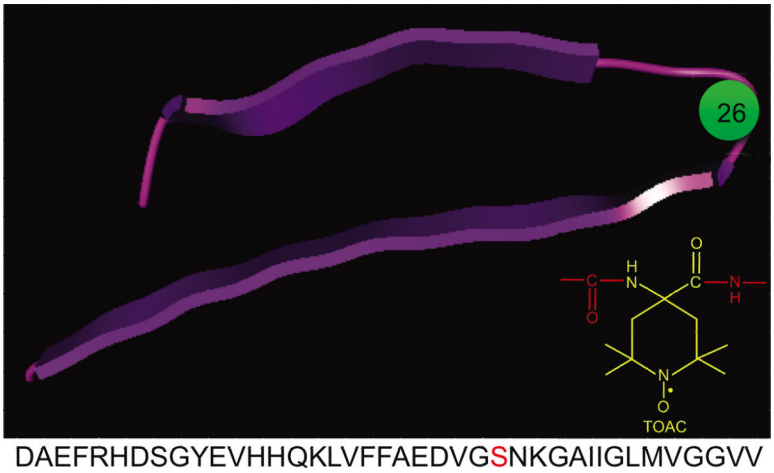

Figure 1.

Location of TOAC label in $A\beta_{(1\text{-}40)}$. Aβ reporter molecule carrying the TOAC nitroxide spin label in place of Ser26. Position 26 lies within a putative hairpin loop connecting the terminal domains of the peptide. The sequence of $A\beta_{(1\text{-}40)}$ is shown below. The position of the TOAC replacement (Ser26) is highlighted.

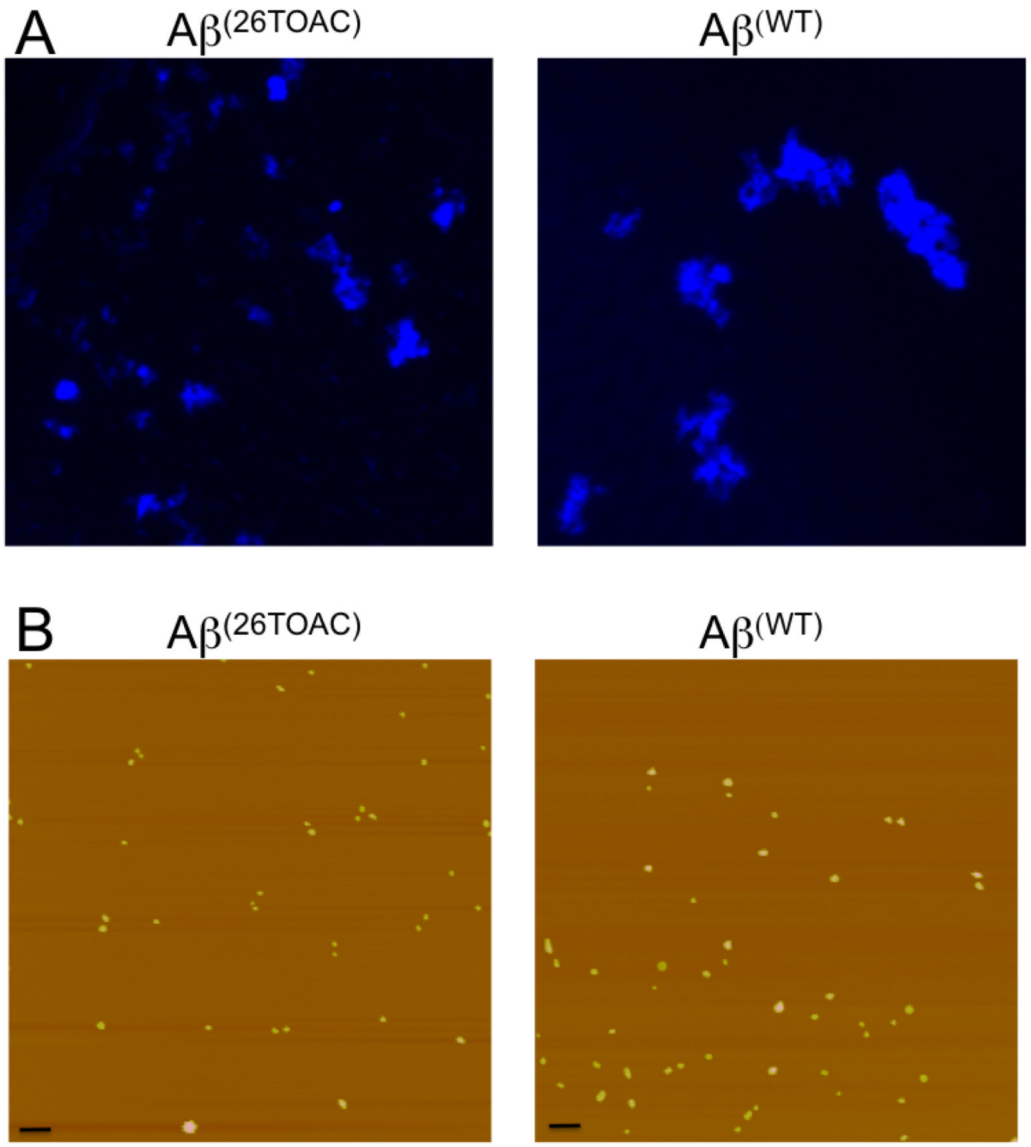

Figure 2.

Aggregation properties of $A\beta^{(26TOAC)}$. (**A**) Small oligomers of $A\beta^{(26TOAC)}$ form fibrillar aggregates as measured by staining with the amyloidophilic dye FSB. This demonstrates that aggregates of TOAC-substituted peptide assume a beta-rich conformation at a similar rate to those formed by native $A\beta_{(1-40)}$. (**B**) The direct visualization of AβO (50 μM) by AFM. The fibrillar aggregates are formed within 1 minute of spotting on mica surface. The scale bars represent 50 nm, with the aggregates of both $A\beta^{(26TOAC)}$ and wt $A\beta_{(1-40)}$ having average diameters in the range of 5-10 nm.

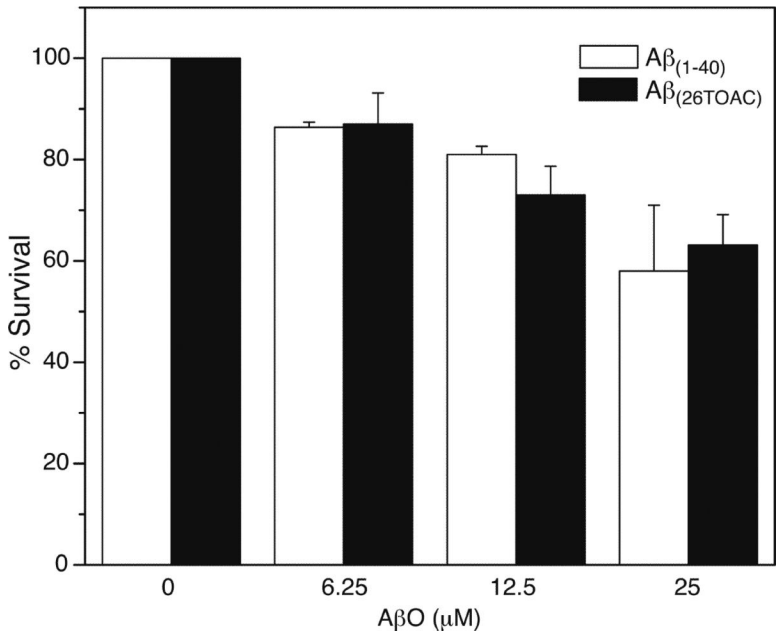

Figure 3.

The cytotoxicity of peptides as determined using a colorimetric MTT (3-(4,5 dimethylthiazol-2yl)-2,5-diphenyltetrazolium bromide) assay for N2a cells treated by $A\beta^{(26TOAC)}$ and native $A\beta_{(1-40)}$.

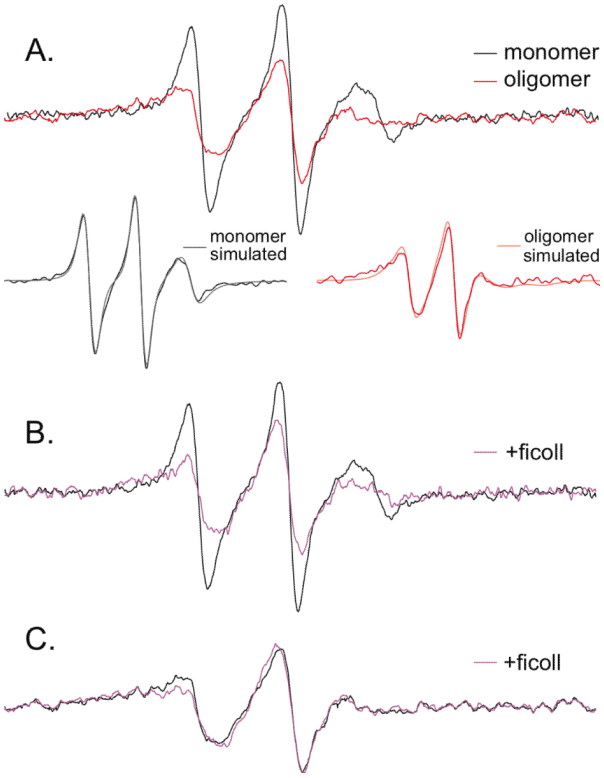

Figure 4.

Dynamics of TOAC-labeled peptide in monomeric or oligomeric samples. In (**A**), the spectrum of monomeric $A\beta^{(26TOAC)}$ is compared to the oligomer. The spectra below compare the individual monomer and oligomer data to simulations generated by the NLSL software as described in Methods. Results for the fit calculate correlation times of 1.3 nsec and 7.1 nsec for the monomer and oligomer, respectively. The viscosity effect on the signals of monomeric (40μM in DMSO) or oligomeric (40μM in PBS) $A\beta^{(26TOAC)}$ are shown in (**B**) and (**C**), respectively. To reduce the likelihood of dipolar broadening between neighboring spins, samples contained 1 part $A\beta^{(26TOAC)}$ to 3 parts native $A\beta_{(1-40)}$.

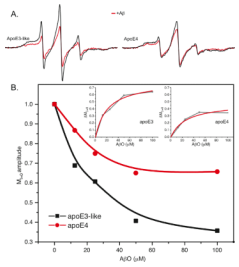

Figure 5.

Isoform differences in AβO binding from the perspective of lipid-free apoE spin labeled at position 264. (**A**) Mixtures contained 30 μM of apoE isoform and 100 μM of oligomeric $A\beta_{(1\text{-}40)}$. The samples were incubated for one hour at 37 °C and scanned by EPR. (**B**) Dependence of the spin-labeled apoE $M_{I=0}$ line intensity (normalized to the intensity in the absence of ligand) on AβO concentration. *Insets*: non-linear regression fits of the titration treated as a binding hyperbola are shown in the insets with the y-axis representing the change in the central line width's intensity (ΔI). Fits to the equation $\Delta I = \Delta I_{max} * L/(K_D + L)$ produced values of ΔI_{max} of 0.79 and 0.48 and apparent K_D values of 21 and 27 μM, respectively.

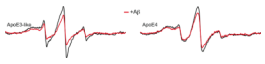

Figure 6.

Isoform differences in AβO binding from the perspective of lipid-bound apoE spin labeled at position 264. Spin-labeled apoE3 and apoE4 (0.5 mg/ml) were bound to human plasma lipids three hours postprandial through a 1 hr incubation at 37 °C. Plasma Lipids (3 hours) on E3 and E4. EPR spectra were then collected for the samples +/- addition of AβO (100 μM).

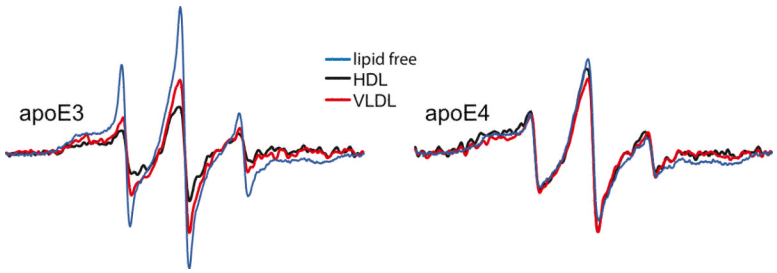

Figure 7.

Isoform differences in AβO binding in the presence of HDL and VLDL. ApoE (30 μM) containing a spin label at position 264 was combined with HDL or VLDL (850 mg/dL) and then oligomeric $A\beta_{(1\text{-}40)}$ (100 μM) was added to the mixture and incubated for one hour at 37 °C, followed by EPR spectroscopy.

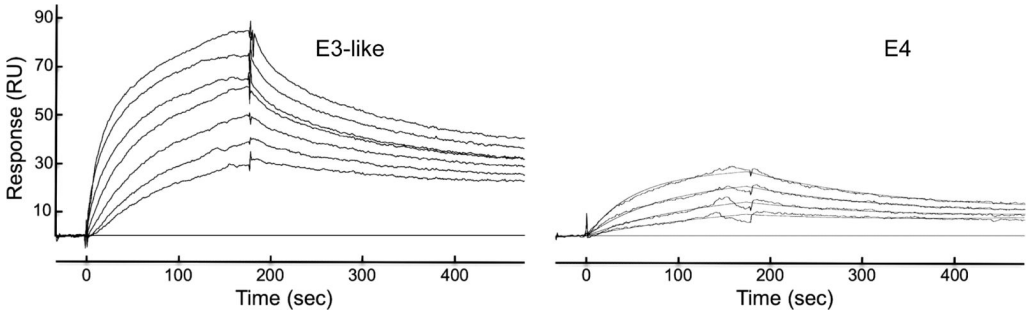

Figure 8.

SPR sensorgrams for the E3-like protein (left) and apoE4 (right) binding to immobilized AβO. Flow concentrations of apoE ranged from 0.2 to 2 μM in PBS pH7.4. Values for K_D (M) were obtained by calculating kd(s^{-1})/ka($M^{-1}s^{-1}$) using Scrubber software. K_D parameters for apoE3-like and apoE4 are $2.66*10^{-8}$ M and $9.77*10^{-8}$ M, respectively.

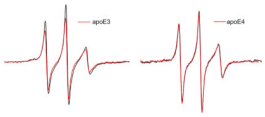

Figure 9.

Spin-labels attached to Aβ monomer also indicate a higher affinity for the E3 isoform. Addition of apoE3 (30 μM) induces a broadening of the spectra reported by spin label at position 26 Aβ in a 40 μM sample of Aβ containing 1 part $A\beta^{(26TOAC)}$ to 3 parts native $A\beta_{(1-40)}$ that was scanned immediately after introduction into aqueous buffer. Addition of apoE4 had no significant effect on the $A\beta^{(26TOAC)}$ spectrum.